EARTH SURFACE PROCESSES AND LANDFORMS
Earth Surf. Process. Landforms **44**, 144–159 (2019)

Published online 20 September 2018 in Wiley Online Library
(wileyonlinelibrary.com) DOI: 10.1002/esp.4488

Debris-flow release processes investigated through the analysis of multi-temporal LiDAR datasets in north-western Iceland

Costanza Morino,[1]* Susan J. Conway,[2] Matthew R. Balme,[3] John Hillier,[4] Colm Jordan,[5] Þorsteinn Sæmundsson[6] and Tom Argles[1]

[1] School of Environment, Earth and Ecosystem Sciences, The Open University, Walton Hall, Milton Keynes MK7 6AA, UK
[2] CNRS UMR 6112 Laboratoire de Planétologie et Géodynamique de Nantes, Université de Nantes, 2 rue de la Houssinière, 44322 Nantes, France
[3] School of Physical Science, The Open University, Walton Hall, Milton Keynes MK7 6AA, UK
[4] Department of Geography, Loughborough University, Loughborough LE11 3TU, UK
[5] British Geological Survey, Environmental Science Centre, Keyworth, Nottingham NG12 5GG, UK
[6] Department of Geography and Tourism, University of Iceland, Askja, Sturlugata 7, IS-101 Reykjavík, Iceland

Received 12 July 2017; Revised 25 July 2018; Accepted 12 August 2018

*Correspondence to: Costanza Morino, School of Environment, Earth and Ecosystem Sciences, The Open University, Walton Hall, Milton Keynes, MK7 6AA, UK. E-mail: costanza.morino@open.ac.uk

ESPL
Earth Surface Processes and Landforms

ABSTRACT: Debris flows are fast-moving gravity flows of poorly sorted rock and soil, mixed and saturated with water. Debris-flow initiation has been studied using empirical and experimental modelling, but the geomorphic changes, indicative of different triggering processes, are difficult to constrain with field observations only. We identify signatures to distinguish two different debris-flow release styles by integrating high-resolution multi-temporal remote sensing datasets and morphometric analysis. We analyse debris flows sourced above the town of Ísafjörður (Iceland). Two debris-flow triggering processes were previously hypothesised for this site: (i) slope failure, characterised by landslides evolving into debris flows; and (ii) the fire-hose effect, in which debris accumulated in pre-existing, steep-sided bedrock passages is transported by a surge of water. It is unknown which process dominates and determines the local risk. To investigate this question, we compare airborne LiDAR elevation models and aerial photographs collected in 2007 with similar data from 2013. We find that two new debris-flow tracks were created by slope failures. These are characterised by steep sliding surfaces and lateral leveed channels. Slope failure also occurred in two large, recently active tracks, creating the preparatory conditions for the fire-hose effect to mobilise existing debris. These tracks show alternating zones of fill and scour along their length, and debris stored below the source-area at rest angles >35°. Our approach allows us to identify and quantify the morphological changes produced by slope failure release process, which generated the preparatory conditions for the fire-hose effect. As debris flows are rarely observed in action and morphological changes induced by them are difficult to detect and monitor, the same approach could be applied to other landscapes to understand debris-flow initiation in the absence of other monitoring information, and can improve the identification of zones at risk in inhabited areas near hillslopes with potential for debris flows.

KEYWORDS: debris flow; release styles; LiDAR; multi-temporal analysis; NW Iceland

Introduction

Debris flows are rapid (e.g. 0.8–28 m s^{-1}; Rickenmann, 1999) and potentially destructive mass movements composed of a cohesionless mixture of water and poorly sorted sediments (Iverson, 1997). To initiate, debris flows require the availability of unconsolidated material, excess moisture to saturate and mobilise this material, and slopes greater than 15°–20° (Costa, 1984; Terzaghi *et al.*, 1996; Rickenmann, 1999; Imaizumi *et al.*, 2006). Hundreds of thousands of cubic metres of sediment can be transported for distances of over tens of kilometres, even on moderate (~5–10%) gradients (Iverson, 1997; Rickenmann and Koschni, 2010). They are distinct from other forms of landsliding due to their periodic occurrence on established paths, usually in gullies or first- order drainage channels (Hungr *et al.*, 2014).

Debris flows can initiate in several ways, e.g. by shallow translational or rotational sliding (Innes, 1983; Costa, 1984), by the erosion and mobilisation of accumulated material on hillslopes or in pre-existing depressions (Davies, 1986; Cannon *et al.*, 2001), or by sediment entrainment in channels (Hungr *et al.*, 2005). Different styles of triggering and propagation

processes of debris flows have inherently different preconditioning factors. It is important to understand which triggering processes (or combination of processes) are active during the formation and evolution of debris flows to anticipate their behaviour in zones exposed to their hazard, and hence to design mitigation and prevention measures.

Direct observation of the initiation processes of debris flows is the best way to identify them, but is seldom possible. In recent years, the development of high-resolution topographic data from laser scanning (or "LiDAR", Light Detection And Ranging) and photogrammetric datasets has facilitated the study of debris flows. Monitoring of debris flows through multi-temporal LiDAR data is becoming more and more common, particularly for sediment budget analysis and for studying debris-flow initiation (Scheidl *et al.*, 2008; Bull *et al.*, 2010; Blasone *et al.*, 2014; Bossi *et al.*, 2015; Cavalli *et al.*, 2017). Bremer and Sass (2012) used a combination of terrestrial laser scanning (TLS) and airborne laser scanning (ALS) to quantify and map the sediment volume transported by a single debris-flow event in the Austrian Alps. Erosion and deposition generated by channel-bed entrainment of sediments by debris flows in the Swiss Alps have been calculated by differencing two ALS digital elevation models (DEMs) (Frank *et al.*, 2015). Loye *et al.* (2016) used time series TLS data to quantify the sediment budgets of two debris-flow events in the Manival catchment (France). They were able to distinguish between the seasonal debris recharge produced by rockfall in winter, and the debris produced by hillslope sediment reworking in spring and autumn. In the same area, Theule *et al.* (2015) used TLS to quantify erosion and deposition caused by debris flows, and ALS to detect unstable sediment deposits that could be a source for new events. In all these studies, the number of the debris-flow events was known and the debris-flow catchments were monitored by other means. However, when catchment changes are not easily identifiable – in the absence of monitoring systems or witnesses – knowing how and when individual or multiple debris-flow events occur is challenging. A possibility that has not been fully explored in literature is the identification and quantification of different debris-flow release processes from multi-temporal laser altimetry datasets, in which the conditions for their development are poorly monitored.

Here, we investigate how two debris-flow initiation processes (slope failure and fire-hose effect, which have been previously proposed for our study area in the Westfjords of Iceland; Decaulne *et al.*, 2005; Conway *et al.*, 2010) manifest themselves in terms of geometric properties and geomorphological features recognisable and measurable in remote sensing data. Specifically, we quantify the geomorphic effects of debris flows on the slope above the town of Ísafjörður through the comparison of two repeat aerial photograph and airborne laser altimetry datasets from 2007 and 2013. In particular, we use the airborne LiDAR data to calculate the volumes eroded and deposited along debris-flow tracks by potential multiple debris-flow events, and we couple these volume quantifications with the analysis of changes in slope and geomorphic observations and interpretations from the aerial photographs. This allows us to assess and distinguish the role of two release mechanisms in debris-flow generation: slope failure and fire-hose effect.

Identifying and characterising different debris-flow processes is useful for understanding both sediment cascades and the implications of the potential hazard posed by debris flows where they occur near inhabited areas. This can be achieved by LiDAR differencing, which in our case has permitted the detection and quantification of debris accumulated at high gradients without the assistance of any other monitoring system or information on the evolution of the hillslope. From remote sensing interpretation alone, we do not know if one or several debris-flow events have mobilised the material between 2007 and 2013 in the tracks that we analyse, but this debris could be the source-material for potentially larger debris flows in the future. This kind of study, implemented with *in situ* channel survey and monitoring, can improve both our understanding of how debris flows develop and mitigate the risks associated with them.

Debris-flow activity in the study area

Slopes in the north-western region of Iceland, the Westfjords (Figure 1(A)), are prone to debris flows (Decaulne, 2005). Ísafjörður is the largest town of the peninsula, with a population of approximately 2600 inhabitants over an area of 4.2 km^2 in 2016. It has more than 150 buildings (including a hospital, two schools, two elderly residences, and three kindergartens) less than 50–300 m from recently emplaced debris-flow runout deposits. Although in this century debris flows have not caused major loss of life in the Westfjords, they do pose a serious hazard to local infrastructure and population (Decaulne, 2004). In mid-June 1999, six debris flows occurred after a sudden and intensive snowmelt period on the slope overlooking the town of Ísafjörður, damaging houses and infrastructure (Decaulne *et al.*, 2005). Moreover, at least 24 debris-flow events occurred on this slope between 1900 and 1999, giving a return period for debris flows of 4–5 years (Decaulne *et al.*, 2005).

Our study site is located above the town of Ísafjörður in the Gleiðarhjalli area, situated on the western side of the Skutulsfjörður fjord (Figure 1(A)). The fjord was shaped by Pleistocene-age glaciers and is carved into the Tertiary Basalt Formation, comprised of 2 to 30 m thick jointed basaltic lava flows separated by lithified sedimentary horizons (from a few centimetres up to tens of metres thick; Thordarson and Hoskuldsson, 2002), which are gently dipping towards the south-east (Kristjánsson *et al.*, 1975; Sæmundsson, 1980).

The Gleiðarhjalli bench, which is located on the south-eastern side of Eyrarfjall Mountain at a height of 470 m above sea level (a.s.l.) on average, is 1500 m long and 450 m wide at maximum (Figure 1(B)). Deposits of poorly sorted glacial till 20–35 m thick (surveyed and measured by visual inspection in the field) are perched on this bench (Figure 2(A)), at whose margin they are unstable. The till deposits are composed of subangular to subrounded clasts varying in size from pebbles to metre-scale boulders and lying in a matrix of clay, silt and sand. The deposits are covered by centimetre to metre-sized angular clasts from talus deposits, which are either lying scattered on the bench or leaning against the rockwall (Figure 2(B)). Chutes (i.e. steep-sided passages scoured in bedrock along which the debris flows can move) are incised into the exposed rockwall at the edge of the bench (Figure 2(B)), forming areas through which most of the transfer of sediment to the lower parts of the slopes takes place.

The SE-facing hillsides above Ísafjörður have steep slopes in the range 25° to 35°, and slightly concave profiles. Below the exposed rockwall, the slope is covered by talus material and relict debris-flow deposits (Figure 2). Grass, moss and patches of dwarf birches and bilberries (30–40 cm high) cover the slope of Ísafjörður on its lower part. Trees are absent, apart from two small artificially forested areas at the foot of the slope (covering ~43 000 m^2 and 6800 m^2, respectively), planted with spruce (3–4 m high on average) as wind-breaks and for aesthetic reasons. The lack of substantial vegetation in the upper part of the slope favours erosional processes (Elwell and Stocking, 1976; Wells, 1981, 1987).

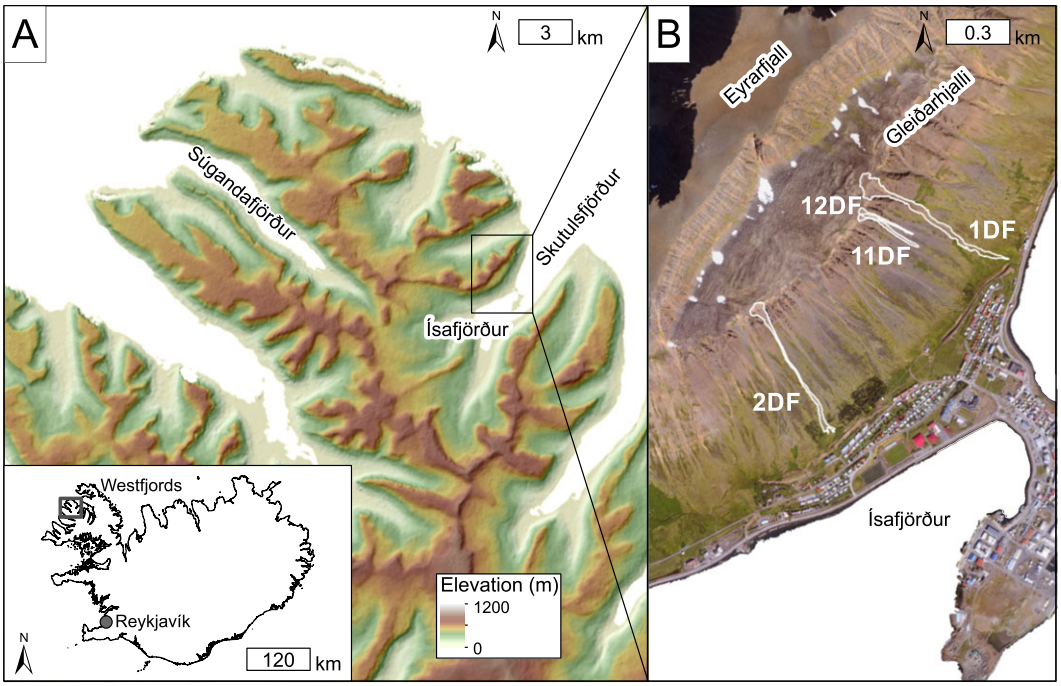

Figure 1. (A) The study area in the Icelandic Westfjords. Elevation data are from the Digital Elevation Model over Europe (EU-DEM) from the Global Monitoring for Environment and Security service for geospatial reference data access project (GMES RDA). (B) Aerial photograph shows the town of Ísafjörður, with debris flows analysed in this study marked with white outlines. [Colour figure can be viewed at wileyonlinelibrary.com]

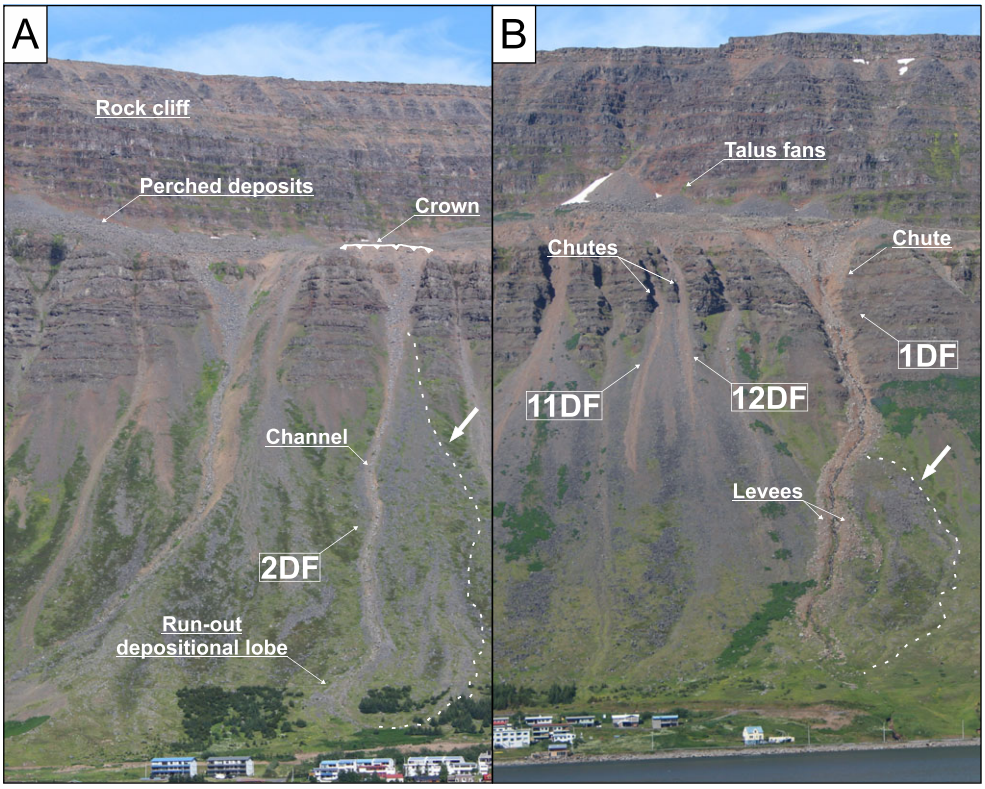

Figure 2. South-east flank of the Eyrarfjall mountain above the town of Ísafjörður showing the four debris-flow tracks analysed for this study (debris flow 2DF in (A), debris flows 1DF, 11DF and 12DF in (B)). Above the rock cliff it is possible to observe talus fans and perched deposits on the Gleiðarhjalli bench; chutes are scoured in the bedrock below the bench ridge and the debris flows' channels incise the deposits from talus material and relict debris flow deposits. Arrows and dashed lines indicate the migration of the channels of 1DF and 2DF in the terminal parts, leaving fan-shape debris accumulation. Some of the runout depositional lobes reach the inhabited areas. The white dotted line marks an example of chute area, the white indented line an example of crown overlying the main failure scarp. Photograph taken on July 26, 2013. [Colour figure can be viewed at wileyonlinelibrary.com]

In Ísafjörður, heavy and prolonged rainfall and rapid snowmelt have been recognised as the main factors that promote rapid mass wasting phenomena, which are also favoured by the steepness of the slope (Decaulne and Sæmundsson, 2003, 2007; Sæmundsson *et al.*, 2003). However, the exact physical mechanisms by which debris flows are initiated have been

hypothesised but not studied in too much detail. This is partially due to the difficulties in accessing and observing the phenomena directly, which is only rarely possible in Ísafjörður (Decaulne *et al.*, 2005), and other mountain environments (Berti *et al.*, 1999; McArdell *et al.*, 2007; Coe *et al.*, 2008).

Among the many possibilities, two processes are most commonly considered responsible for triggering debris flow here: slope failure and the fire-hose effect (Decaulne *et al.*, 2005; Conway *et al.*, 2010). Initiation by slope failure is characterised by one or more discrete slope failures, instigated by changes in pore water pressure due to gradual *in situ* infiltration of rain or snowmelt (Hungr *et al.*, 2001). As failure proceeds, contraction of debris causes an excess in pore water pressure, weakening the debris mass and resulting in the transformation from localised failure into a debris flow (Iverson, 1997). It is believed that this initiation style is experienced in the Gleiðarhjalli area; Decaulne *et al.* (2005) observed that intense precipitation and snowmelt caused saturation of the debris mantle covering the bench. Decaulne *et al.* (2005) further observed that the debris flows begin with rockfalls originating from the edge of the bench. This implies a subsequent loss of support, leading to the perched deposits sliding and then forming channelised debris flows. The authors report that, between the rock-fall phase and the debris-flow phase, the uppermost part of the tracks were temporarily blocked by the collapsed material from upslope, being prone to be re-mobilised by further events.

Initiation by the fire-hose effect (Johnson and Rodine, 1984) is characterised by a concentrated flow of water that entrains loose deposits, which are generally located in a steep bedrock channel, torrent or chute (Godt and Coe, 2007). An increase in pore-water pressure results in their conversion into a debris flow (Johnson and Rodine, 1984; Coe *et al.*, 1997; Griffiths and Webb, 2004). The recurrence interval of such flows is controlled by the debris accumulation rate in the source area and the timing of triggering precipitation. The fire-hose effect has been inferred to have been active in the Westfjords based on field inspections (Decaulne and Sæmundsson, 2006; Conway *et al.*, 2010), but has never been fully characterised and quantified.

Methods

Dataset-processing and Digital Elevation Model generation and interpolation

In 2007 and 2013, the UK Natural Environment Research Council's Airborne Research Facility Data Analysis Node (NERC-ARF-DAN) collected aerial photography and LiDAR data for Súgandafjörður and Skutulsfjörður areas in Iceland. Details of both aerial surveys are reported in Table I. As the methods of remote sensing data collection differed between the two years, including the location/type of the reference GPS base stations on the ground, the two LiDAR datasets needed further processing to attain a satisfactory comparison. Alignment and filtering are required when comparing different types of datasets, in order to achieve sufficient accuracy for producing volumetric differencing (Bremer and Sass, 2012; Roberti *et al.*, 2017). Furthermore, co-registration error between flightlines needs to be corrected. Approaches such as morphometric parameter distributions (Sofia *et al.*, 2013) or spatially variable error models (Schaffrath *et al.*, 2015) have been developed to correct these errors. Fuzzy inference system (Fis) has also been used to estimate the spatial variability of elevation uncertainty in individual DEMs, in order to propagate the uncertainties into the so-called DEM of Differences (DoD) map (Moss, 2000; Scheidl *et al.*, 2008; Theule *et al.*, 2012; Blasone *et al.*, 2014; Bossi *et al.*, 2015), and then assess the significance of the propagated uncertainty (Wheaton *et al.*, 2010; Bangen *et al.*, 2016; Cavalli *et al.*, 2017). The iterative closest point (ICP) algorithm has successfully been used to improve co-registration errors where data from individual flightlines can be used (Besl and McKay, 1992; Chen and Medioni, 1992; Zhang, 1994). The correction is based on a least squares adjustment (similar to that of Akca, 2007), which matches the surface shape between each track to individually align the tracks relative to a reference point cloud (Brasington *et al.*, 2000; Lane *et al.*, 2003; Milan *et al.*, 2007). The ICP procedure allows the alignment between two point clouds to be as close as possible (James and Robson, 2014; Micheletti *et al.*, 2015). Since we have reliable LiDAR data collected in 2013, and we could use this as the reference elevation dataset for aligning the 2007 LiDAR flightline (s), we chose to apply ICP procedure. In order to assess the DEM accuracy, we assumed the propagated DEM uncertainty in the DoD as uniform, and determined a minimum level of detection, above which changes were considered to be real (Brasington *et al.*, 2000, 2003; Fuller *et al.*, 2003). This approach has been successfully used in recent analogue case studies (Bossi *et al.*, 2015; Cavalli *et al.*, 2017).

The 2007 LiDAR point data have horizontal and vertical shifts of up to 2 m between flightlines caused by a lack of between-track corrections in the initial processing (such errors are particularly problematic in steep terrain, see Favalli *et al.* (2009) for a full analysis). The 2013 data by comparison have averagely 6 cm vertical and horizontal differences between overlapping flightlines. We used only one flightline from the 2007 LiDAR data and cropped out the area of interest in order to reduce the errors from the LiDAR data processing. Cropping the dataset into a relatively short along-track segment (1.5 km) reduces the errors introduced by poorly integrated flight navigation and positional information. We then corrected the misalignment between the 2013 and 2007 datasets by means of the open source CloudCompare software, using an implementation of the ICP algorithm. We used the point cloud from the 2013 LiDAR data as the reference data for the 2007 data, as the 2007 cloud had more severe co-registration issues. Once corrected, the mean value of the normal distances of the 2007 point cloud from the 2013 reference is 0.49 m (standard deviation 0.28 m); from the value of 0.49 m we defined our minimum level of detection as ±0.5 m.

After the co-registration, we imported the point clouds into ArcGIS and gridded the LiDAR data at 1 m/pixel, using the return time of the last peak of light to reach the receiver from the LiDAR laser shot, which is generally assumed to be the ground return. To do so, we used the LAStools extension for

Table I. Details of airborne survey of Súgandafjörður and Skutulsfjörður fjords for year 2007 and year 2013

Date of collection	Type of data	Survey instrument	Survey details
05 August 2007	Aerial photography	Leica-Wild RC10	63 photographs
	LiDAR data	Optech ALTM3033	17 lines, 68 M Points, 2.5 points/m^2
12 August 2013	Aerial photography	Leica RCD 105	340 photographs
	LiDAR data	Leica ALS50-II	23 lines, 287 M Points, 1.5 points/m^2

ArcGIS, which temporarily triangulates the LiDAR points into a Triangulated Irregular Network (TIN), and then rasterises the TIN into a Digital Elevation Model. The rasters were constructed so as to be orthogonal, i.e. so that the pixel-size and pixel-centres were the same. Finally, using ArcGIS, we calculated elevation changes and volumes by subtracting the 2007 gridded data from the 2013 data, producing the DoD.

DEM of difference error propagation

Any individual errors in the DEMs derived from the LiDAR, generated during surveying and post-processing, are propagated into the DoD (Goulden and Hopkinson, 2010). The DoD error varies spatially and arises from factors such as steepness of the terrain (causing data-gaps), the growth/change of dense vegetation, the varying density of the point clouds (data-gaps or false-smoothing) or misalignment between datasets (which causes an increase in error with the measurements between different datasets; Reuter *et al.*, 2009). On the majority of the hillslope of Ísafjörður, between 2007 and 2013 there are few changes in elevation above the minimum level of detection (less than 0.5 m vertical change for 89% of the area analysed), and those that do occur are usually caused by noise or artefacts in the data (Figure 3(A)–(D)). Figures 3(A) and (B) show areas with no observable differences in the aerial photographs between 2007 (Figure 3(A)) and 2013 (Figure 3(B)), yet detectable differences in the DoD. Apparent elevation changes of up to ±5 m in the DoD are caused by the steepness of the bedrock cliff – where different (sub-pixel) horizontal positions of the laser spots between years result in large differences in the height values. Artefacts with a magnitude of ±2.5 m can be caused by growth and/or changes in vegetation, but such example can be easily identified by comparison with the aerial photographs (Figure 3(C)–(D)).The deposited and eroded volumes along and within the debris-flow tracks are key metrics in this study, so we explicitly derived the effects of errors on our volume calculations, using the DoD to determine the relative absolute and percentage errors in the estimates (Table II). First, we manually selected areas lacking visible change from aerial photographs ('stable areas') and with similar setting (i.e. slope angles and vegetation/materials) to the analysed debris flows, and we calculated their volume changes. We then divided the volumes of the sampled debris flows obtained from the DoD by the area of the selected zones that showed no changes in the aerial images, and multiplying the results by the area of the sampled debris flows. The volume error calculated with this approach depends on the scale of the process (when the uncertainty on the measurements have minimum values, errors are not proportional to the measurement), so errors are low for medium-scale flows (volumes between 1000 and 100 000 m^3; Innes, 1983), ranging between ±3% and ±5% for deposited volumes and ±4% for eroded volumes. Small-scale flows (volumes of 1–1000 m^3; Innes, 1983) often have higher relative error because they cover smaller areas and mobilise less material, giving calculated errors of ±9–11% for deposited volumes and ±5–7% for eroded volumes. Particularly high values of error occur where small volume flows cover large spatial areas. Furthermore, some of the error values for volumes are relatively large (see Table II), because we have used a fixed vertical uncertainty, so zones whose volume values are dominated by vertical changes with magnitudes close to that of the minimum level of detection (±0.5 m) have large percentage errors.

Track selection, naming and segmentation

We studied four debris-flow tracks on the slope above Ísafjörður (Figure 1(B)). We adopted and extended the naming protocol

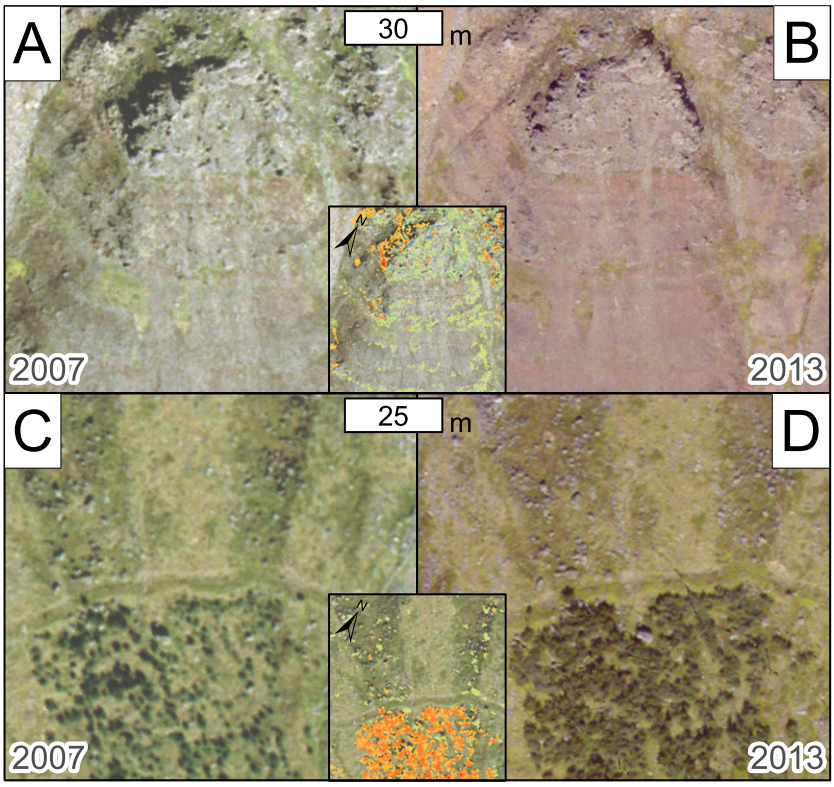

Figure 3. Aerial photographs from 2007 (left side) and 2013 (right side) of a portion of the steep cliff above Ísafjörður (A, B) and of the forest on ESE side of the town (C, D) showing different sources of noise in the map of difference in elevation (in the centre, see Figure 5 for legend). Noise has been cleaned by checking for changes in the aerial photographs and distinguishing the signal. [Colour figure can be viewed at wileyonlinelibrary.com]

Table II. Results of the measured eroded and deposited volumes and other parameters of debris flows

Debris flow ID		Erosion (m^3)	Error (m^3)	Error (%)	Deposition (m^3)	Error (m^3)	Error (%)	Area (m^2)	Maximum lenght (m)	Chute width (m)	Elevation drop (m)
Debris flow 1DF		8552	± 322	± 4	4079	± 223	± 5	23952	803	125	406
Subareas ID	1DFa	5622	± 132	± 2	629	± 91	± 15	9845	168	-	-
	1DFb	256	± 31	± 12	2234	± 21	± 1	2300	129	-	-
	1DFc	2674	± 159	± 6	1216	± 110	± 9	11807	506	-	-
Debris flow 2DF		5001	± 183	± 4	3760	± 127	± 3	13596	727	74	411
Subareas ID	2DFa	3601	± 28	± 1	63	± 19	± 31	2077	51	-	-
	2DFb	201	± 43	± 22	3058	± 30	± 1	3225	156	-	-
	2DFc	1198	± 111	± 9	639	± 77	± 12	8294	520	-	-
Debris flow 11DF		862	± 46	± 5	339	± 32	± 9	3394	325	29	235
Subareas ID	11DFa	832	± 31	± 4	70	± 21	± 30	2303	187	-	-
	11DFb	30	± 15	± 49	269	± 10	± 4	1091	138	-	-
Debris flow12DF		628	± 42	± 7	271	± 29	± 11	3131	286	32	207
Subareas ID	12DFa	549	± 24	± 4	82	± 16	± 20	1777	137	-	-
	12DFb	78	± 18	± 23	188	± 13	± 7	1354	149	-	-

for debris-flow tracks used in Conway *et al*. (2010), who studied debris flows in the same area. They named 10 debris-flow tracks using numbers from 1 to 10 followed by the acronym 'DF'. As two of the debris-flow tracks coincide with two tracks analysed in this study, namely debris flows 1DF and 2DF, we used those names. We continued the same numbering system for two newly developed debris flows: debris flows 11DF and 12DF (Figure 1(B)).

We selected these four tracks because they show substantial (>±0.5 m) geomorphic changes between 2007 and 2013 in the differenced LiDAR datasets. These include morphological changes in the chutes at the front edge of the Gleiðarhjalli bench and in the upper part of the channels. We focused our analysis at these locations, being the zones of the debris flows where the majority of the changes occurred. Two of the four tracks, 11DF and 12DF (Figure 2(B)), did not exist in the 2007 data. The other two, 1DF and 2DF tracks (Figure 2(A)–(B)) were already present in 2007, but they had changed their form by 2013. Because 1DF and 2DF are different from 11DF and 12DF in their size, morphology and the processes that controlled their formation (as discussed below), we treat the two pairs of debris flows separately in the 'Results' and 'Discussion' sections.

Having differenced the LiDAR datasets, we observed that, within the four debris-flow tracks, elevation changes occur in clearly defined, down-flow spatial domains. Since the debris-flow tracks present an atypical distribution of volumes, we segmented them and outlined different subareas according to the predominance of negative or positive elevation change from visual inspection; for example, negative elevation change was predominant in the upper part of 2DF track, so we split it from the strongly contrasting area below, characterised by a positive change in elevation (see Figure 5(A) in 'Results' section). This in turn allowed us to calculate the eroded and deposited volumes for these subareas and for the debris-flow tracks as a whole (see Table II in 'Results' section).

2007–2013 comparison

To analyse the changes occurring along each debris-flow track, we adopted the following approaches:

(i) to evaluate the deposited and eroded volumes within each debris-flow track, we derived the volumetric changes in these zones (i.e. debris-flow tracks and debris-flow subareas);
(ii) we visually identified geomorphological changes that occurred along the tracks in aerial photographs. Additionally, we performed repeated field observations (summer 2012, 2013, 2016) in order to check what we observed and mapped from remote sensing;
(iii) we created a slope map at 1 m/pixel using the standard tools provided in Spatial Analyst of ArcGIS; the slope angle was derived using the steepest downhill slope as calculated by fitting a plane through the eight nearest neighbours (neighbourhood slope algorithm, also known as the average maximum technique; Burrough *et al*., 2015). Slope was evaluated for each subareas of the four debris flows: we took topographic profiles along the line of steepest descent, then extracted both the elevation values and the slope values for both the 2007 and 2013 DEMs along those lines.

Results

Morphology and morphometry of debris-flow tracks 1DF and 2DF

1DF and 2DF are the largest debris-flow tracks analysed in this study, having mobilised volumes up to 14 times larger over areas up to 8 times wider than 11DF and 12DF (see dimensional details in Table II). They are deeply incised and have chutes carved in bedrock in their upper part, with channels cutting slope deposits (Figure 2). In their terminal parts it is possible to observe fan-shaped debris accumulations (Figure 2). Over the whole debris-flow tracks, total erosion volumes are larger than their total deposition volumes. 1DF has an erosion volume more than twice the depositional volume, while 2DF has 25% less deposition than erosion over the whole volume mobilised (see Table II). The net sediment budget should be near zero, but the deposits of the terminal lobes that reached the defensive protections were removed by the local authorities.

1DFa and 2DFa: most of the erosion in 1DF and 2DF occurs in their upper subareas (designated as 'a'), namely in the perched material at the edge of the bench and in the apical chutes carved into the bedrock. Erosion occurs in subareas 1DFa and 2DFa, amounting respectively to 5622 ± 132 m^3 and 3601 ± 28 m^3 (Figures 4(B) for 1DF, 5(B) for 2DF, Table II), over a great range of slope (Figure 6). For both the debris-flow tracks in the time span between 2007 and 2013, the slope angle below the scarps and in the apical chutes remains on average above 35° (Figure 6(A)–(H), Table III). Erosion is also evident from the morphology of the upper subareas 1DFa and

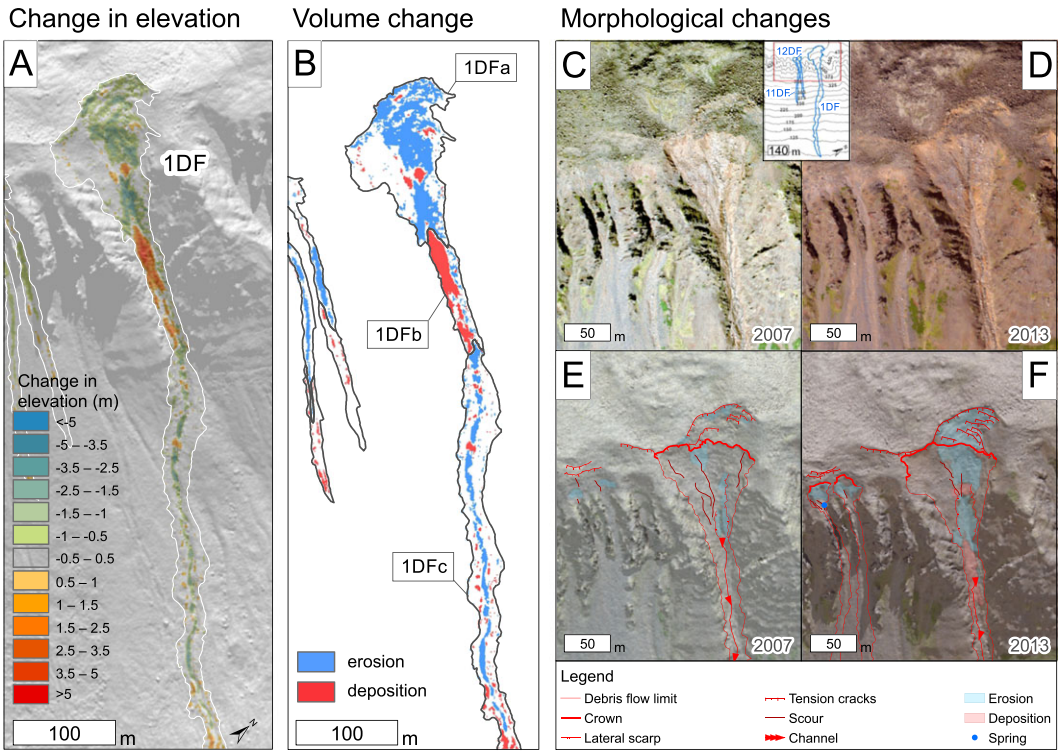

Figure 4. (A) Elevation-difference map of debris-flow track 1DF obtained calculating the difference in elevation that occurred between 2007 and 2013, overlying the hillshade model derived from 2013 LiDAR. (B) Maps of the erosion and deposition distribution of debris-flow track 1DF derived by differencing the LiDAR generated topography from 2007 and 2013. The debris flow was segmented in subareas of prevailing erosion and deposition along its length. Distal lobes extensively modified during protection works (Figure 10) are omitted to avoid confusion. (C-F) Aerial photographs of the upper zones of debris flows 1DF, 11DF and 12DF from 2007 (C) and 2013 (D) compared, with simplified sketches of the main observable features (E and F, where the hillshade models derived from 2007 and 2013 LiDAR data, respectively, are overlain by aerial photographs in transparency). [Colour figure can be viewed at wileyonlinelibrary.com]

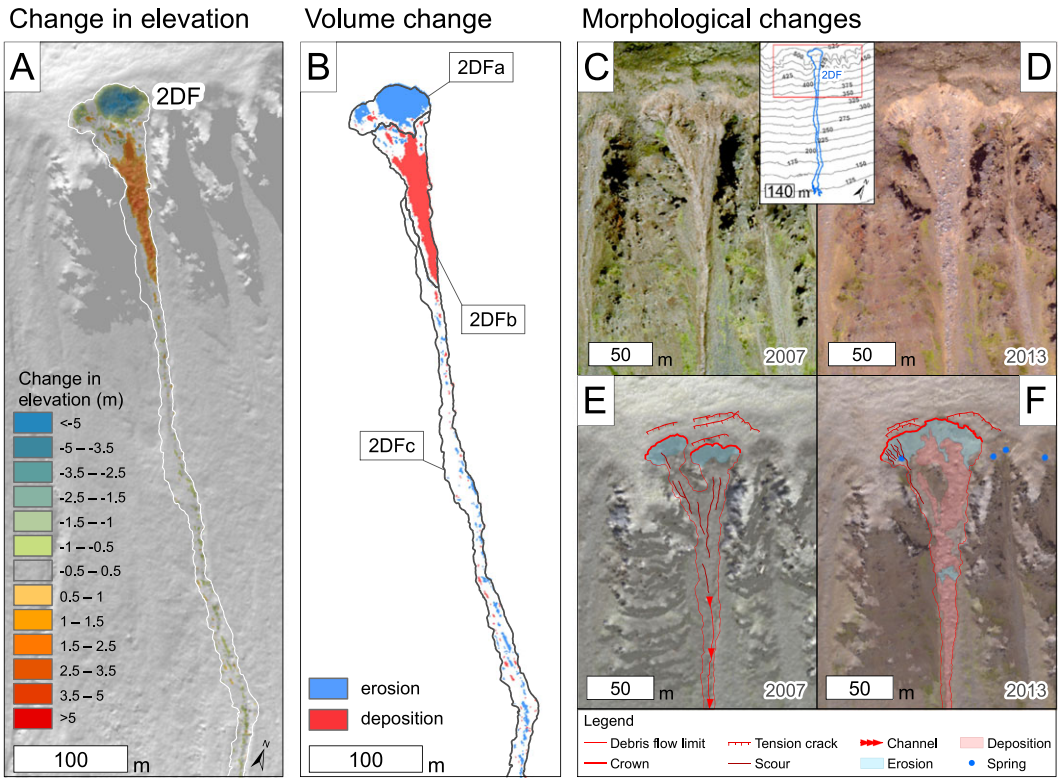

Figure 5. (A) Elevation-difference map of debris-flow track 2DF obtained calculating the difference in elevation that occurred between 2007 and 2013, overlying the hillshade model derived from 2013 LiDAR. (B) Maps of the erosion and deposition distribution of debris flow track 2DF derived by differencing the LiDAR generated topography from 2007 and 2013. The debris flow was segmented in subareas of prevailing erosion and deposition along its length. Distal lobes extensively modified during protection works (Figure 10) are omitted to avoid confusion. (C-F) Aerial photographs of the upper zones of debris flow 2DF from 2007 (C) and 2013 (D) compared, with simplified sketches of the main observable features (E and F, where the hillshade models derived from 2007 and 2013 LiDAR data, respectively, are overlain by aerial photographs in transparency). [Colour figure can be viewed at wileyonlinelibrary.com]

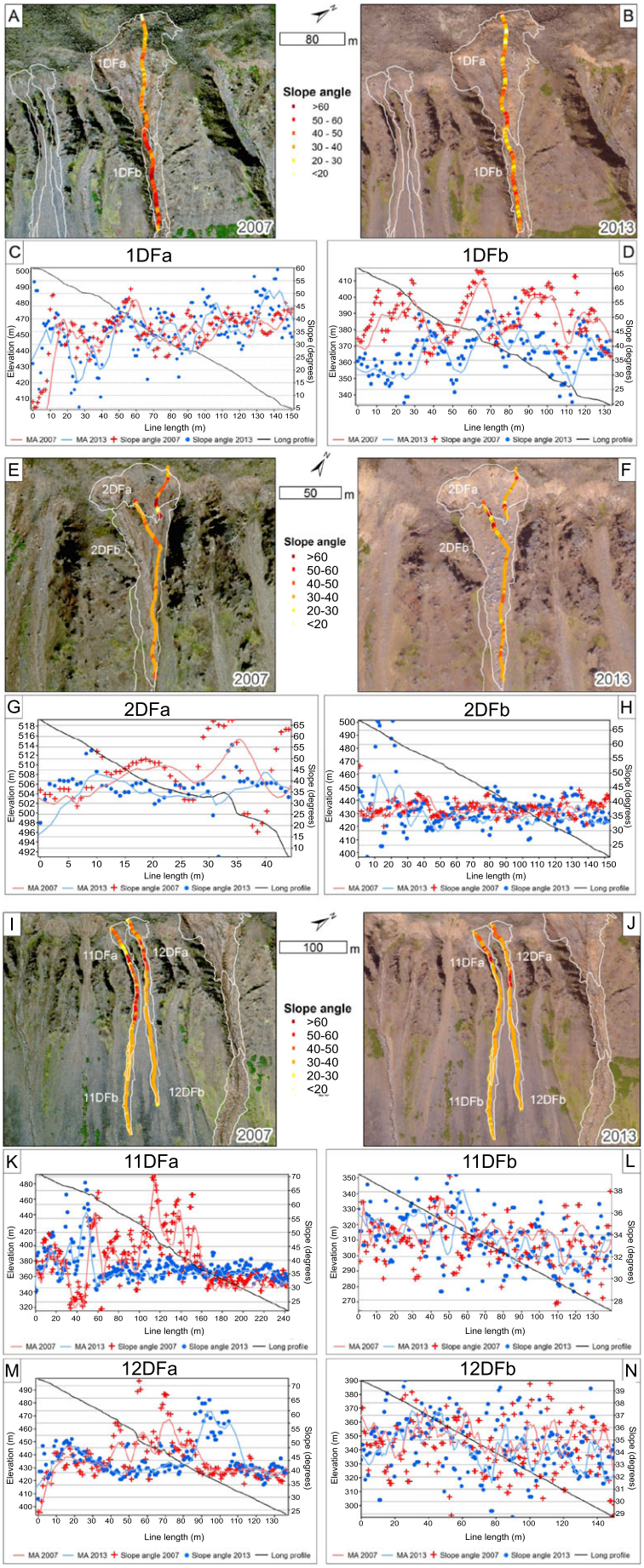

Figure 6. Aerial photographs of the upper zones of debris flows from 2007 (A, E, I) and 2013 (B, F, J) showing the steepest slope lines with colour indicating the slope values. Below, plots of the slope angles from 2007 (in red) and 2013 (in blue) against the long profile representing the terrain elevation in 2013 (black continuous line) for subareas 'a' (C, J, K, M) and 'b' (D, H, L, N). Red and blue continuous lines indicate the moving average (MA, interval 1°) for year 2007 and 2013 respectively. [Colour figure can be viewed at wileyonlinelibrary.com]

Table III. Analysis and uncertainty values for slope angle values plotted on profiles in Figure 6

Debris flow subareas ID	2013			2007		
	Median slope	Mean slope	Standard Deviation	Median slope	Mean slope	Standard Deviation
1DFa	36.91	35.98	±10	37.29	35.33	±8
1DFb	37.96	38	±7	48.83	49.44	±8
1DFc	30.18	30.19	±11	25.83	25.95	±10
2DFa	38.08	37.61	±7	44.21	43.83	±13
2DFb	35.97	37.08	±7	37.34	37.81	±3
2DFc	32.57	31.15	±7	30.73	32.4	±12
11DFa	36.37	37.52	±5	37.58	40.43	±10
11DFb	33.85	33.74	±2	33.33	33.24	±2
12DFa	34.31	40.86	±7	37.1	40.22	±9
12DFb	34.31	34.48	±2	34.65	34.46	±2

2DFa. In 1DFa in 2007, tension cracks, associated with areas of erosion located directly below them, cut the bench above the crown (Figure 4(C), (E)), with three more appearing in 2013, concomitant with enlarged erosion areas (Figure 4(D), (F)). In 2DFa, the main failure scarp in 2013 originated from two already well defined release scarps that since 2007 regressively eroded 22 m (Figures 5(E), (F); note the paler material marking the main scarp below the crown in Figure 5(D)). Tension cracks that are present above the crown in 2DFa in 2007 had been partially erased by regressive erosion by 2013. Springs rise at the contact between the deposits perched on the bench and the underlying bedrock (Figure 5(D), (F)).

1DFb and 2DFb: immediately below 1DFa and 2DFa, positive elevation change of up to ~5 m occurs in the chutes and in the upper channels (Figure 4(A) for 1DF, 5(A) for 2DF). The majority of the accumulated deposits of 1DF and 2DF, 2234 ± 21 $m^3$and 3058 ± 30 m^3 respectively (Table II), lie in these subareas (designed as 'b'). In 1DFb, the slope angle values for 2013 are equal to or less than those of 2007, with deposition occurring at a high slope gradient (mean of 38° in 2013, 49° in 2007, Table III). In subarea 2DFb, slope angle values remained constantly high along the profile between 2007 and 2013 (mean is 37–38°, Table III, Figure 6(E)–(H)). In 1DFb, the aerial images show that new deposits have been transferred into the chute by 2013, obliterating the scours and filling the zones of erosion that were present in 2007 (Figure 4(C)–(F)). In 2DFb, the upper catchment, the chute and the upper channel were largely empty of debris in 2007, whereas by 2013 they are filled by a deposit of blocky material (Figure 5(C)–(F)).

1DFc and 2DFc: further downstream, we have grouped smaller, more discontinuous zones of negative and positive elevation change of up to 1 m in magnitude in the subareas 1DFc and 2DFc (Figures 4(A)–(B) for 1DF, 5(A)–(B) for 2DF). These zones of erosion and deposition do not correspond to the position of the channel and levees, but they alternate along the channel, almost as far downslope as the terminal lobes. Levees are built up in association with discrete zones of erosion. Part of the debris transferred between 2007 and 2013 was deposited here (1198 ± 111 m^3 in 1DFc and 639 ± 77 m^3 in 2DFc, see Table II). In both the subareas, the slope angle values do not greatly vary between 2007 and 2013 (Table III).

Morphology and morphometry of debris-flow tracks 11DF and 12DF

Debris-flow tracks 11DF and 12DF are smaller than 1DF and 2DF (see morphometric properties in Table II). They originate from the edge of the bench, and their channels are only moderately incised into the existing slope deposits. The spatial distribution of negative elevation change extends from the upper catchments, along the chutes and into the upper part of channels newly incised into the slope deposits (Figure 7). 11DF and 12DF tracks are unconstrained by previous levees in their mid-sections and have newly formed levees and depositional lobes in their lower reaches (Figure 7).

11DFa and 12DFa: on the failure scarps, the negative elevation change between 2007 and 2013 is up to 2.5 m, whereas in the chutes and channels it is up to 5 m (Figure 7(A)). Erosion is dominant in these subareas: 832 ± 31 m^3 in 11DFa and 549 ± 24 m^3 in 12DFa (Table II). Both 11DFa and 12DFa erosional subareas (Figure 7(B)) show an anti-correlation in their slope profiles between the two observation dates: low slope values in 2007 match increased slope angle in 2013, and vice versa (Figures 6(I), (K), (M), Table III). Between 2007 and 2013, in both the upper catchments and chutes of 11DF and 12DF the slope angle in the chutes generally remained above 35°. In the 2007 aerial photographs, the presence of tension cracks and material different in colour and with fewer blocks than the surroundings in the scarp area of 11DF indicates that erosion had already occurred (Figure 4(C), (E)). A well-defined main failure scarp and associated erosion are observable in the upper catchments in 2013, and two new channels overlay the coarse grey deposits of the talus slope (Figure 4(D), (F)). Springs rise at the contact between deposit mantle on the bench and the underlying bedrock (Figure 4(D), (F)).

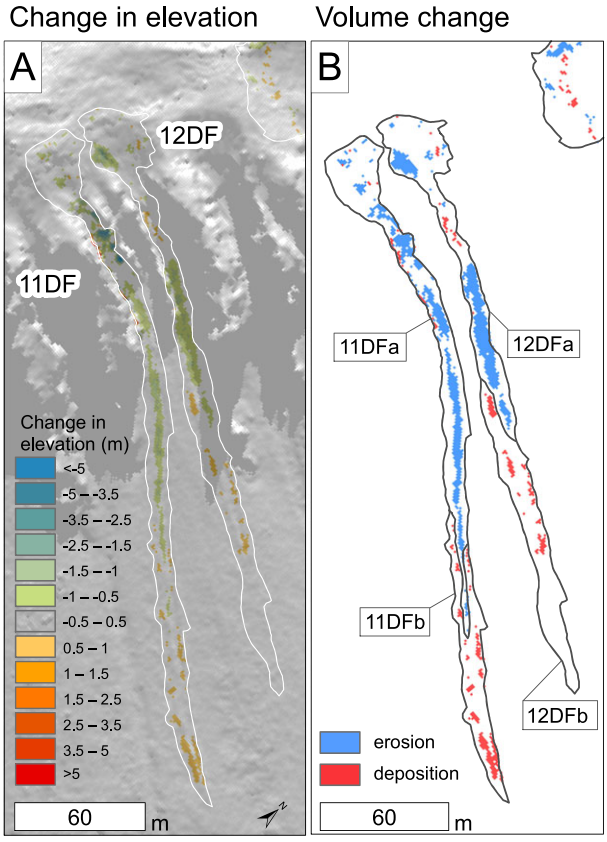

Figure 7. (A) Elevation-difference map of debris-flow tracks 11DF and 12DF obtained calculating the difference in elevation between 2007 and 2013, overlying the hillshade model derived from 2013 LiDAR. (B) Maps of the erosion and deposition volume distribution of debris-flow tracks 11DF and 12DF derived by differencing the LiDAR generated topography from 2007 and 2013. The debris flows were segmented in subareas of prevailing erosion and deposition along their length. [Colour figure can be viewed at wileyonlinelibrary.com]

11DFb and 12DFb: these subareas (Figure 7(B)) show zones of positive elevation change (up to 1 m), and these take the form of slightly outlined lateral levees and a straight terminal lobe (Figure 7(A)). These depositional landforms constitute 269 ± 10 m^3 of material in 11DFb and 188 ± 13 m^3 in 12DFb. The slopes along the steepest profiles of 11DFb and 12DFb show a steady trend with high average values (33°–34°) in both years (Figures 6(J), (L), (N), Table III).

Discussion

Analysis of debris-flow initiation: 11DF and 12DF

A debris flow originates by slope failure when individual failures, or numerous small failures, coalesce, transforming into a debris flow (Fairchild, 1987; Rodolfo *et al.*, 1996; Iverson, 1997). Slope failure-initiated debris flows require the availability of loose material on steep slopes and an accumulation of water in the deposits, so they occur when rainfall and snowmelt cause an increase of pore-water pressures (Sidle and Swanston, 1982; Anderson and Sitar, 1995). This can commonly cause the rise of a water table at the contact of the debris cover with the impermeable bedrock or on top of impermeable layers (Campbell, 1975; Iverson, 1997; Decaulne *et al.*, 2005). In the Westfjords of Iceland, long-duration rainfall and/or snowmelt associated with rain are the two main sources of water for triggering debris flows. For example, extreme rainfall of 63 mm/24 h after 1 month of rainy days (about 140 mm of cumulative precipitation) triggered the debris-flow event in Ísafjörður in September 1996 (Decaulne and Sæmundsson, 2007). Over 40 mm of one month-cumulative precipitation related to snowmelt triggered a debris-flow event in Ísafjörður in June 1999, after a sudden (2 weeks) increase in air temperature from 1 to 4°C to 14–17°C (Decaulne *et al.*, 2005; Decaulne and Sæmundsson, 2007). In Decaulne *et al.* (2005), the initiation for the debris-flow events in Ísafjörður in June 1999 is identified by the appearance of the subsurface runoff at the edge of the Gleiðarhjalli bench, causing erosion of material and generation of rotational slide evolving into debris flows downslope. Debris flows 11DF and 12DF — that were not present at the time of observations made by Decaulne *et al.* (2005) — have these characteristics. Springs coming out between the sediment mantle and the bedrock are visible in aerial images in the scarp of 11DF (Figure 4(D), (F)), showing that runoff could have initiated erosional processes. This is a condition that has been observed in other environments; Bremer and Sass (2012) in the Austrian Alps identified the starting zones of debris flows at the bedrock–debris interface where runoff is concentrated. The combination of springs and loose debris has also been reported in the Alpine environment as one of the most important preparatory factors for slope failure (Marchi *et al.*, 2002; Wieczorek and Glade, 2005). This is a plausible mechanism in Ísafjörður for the weakening and saturation of the deposits, leading to the development of discrete slope failures evolving into debris flows.

Debris flows 11DF and 12DF have a simple morphology: erosion in the upper part (11DFa with 832 ±31 m^3, and 12DFa with 549 ± 24 m^3) and deposition in the terminal part (11DFb with 268 ±10 m^3, and 12DFb with 188 ± 13 m^3). Erosion extends from the edge of the bench, to the chutes, into the newly formed channels on the hillslope. Simple curved main scarps and crown-parallel tension cracks are due to a rotational sliding process (Figures 4(C)–(F), 8(A)). A negative elevation change of up to 5 m in the chute and in the channel shows that, once slope failure started from the front of the bench, it mobilised material that was already in transfer, and with saturation evolved into a debris flow, forming a terminal lobe and lateral levees. Sediment transfer is further evidenced by the fact that in the chutes and upper channels, low slope values in 2007 match increased slope angles in 2013, and vice versa. The entrainment and transport of debris from the chutes and channels is also expected because of their gradient above 35° both in 2007 and 2013. Debris-flow tracks 11DF and 12DF are short: <250 m long.

Our suite of observations and measurements for 11DF and 12DF tracks fits with the characteristics of the slope failure process reported in the literature. Theule *et al.* (2012) used multi-temporal topographic surveying from TLS and ALS to monitor sediment transport by two debris flows in the French Alps. Low rainfall intensity events caused short-runout debris flows (less than 100 m) generated by talus slope failure (magnitude of erosion 266 m^3, magnitude of deposition 268 m^3). Cannon *et al.* (2001) reported ~84 debris flows in Colorado initiated by landslides; they back-traced the debris-flow paths to discrete landslide-scar sources and estimated their volumes, which had a range of ~95 to 2500 m^3. Debris flows in Switzerland have been shown to originate from individual shallow rotational slides on slopes with angles between 25° and 45°, and with volumes of tens to a few hundred cubic metres (Hürlimann *et al.*, 2003). The order of magnitude of the volumes and the size and morphological characteristics of the debris flows analysed in these three studies match well with our quantification and observations of debris-flow tracks 11DF and 12DF (Figure 8(A)).

Analysis of debris-flow initiation: 1DF and 2DF

Material released by slope failure can be transferred into a channelised area. Then, debris can either be transferred downslope, if saturated, evolving into a debris flow, or can cease to be mobile, generating a debris dam and obstructing the channel (Bovis and Jones, 1992; Iverson *et al.*, 2000). Formation of such a debris dam creates the optimal conditions for the development of the fire-hose effect. This mechanism occurs when an overland flow is concentrated by chutes or depressions in the bedrock and becomes a debris flow when impinging on loose debris accumulated in those depressions (Fryxell and Horberg, 1943; Curry, 1966; Johnson and Rodine, 1984; Berti *et al.*, 1999; Coe *et al.*, 1997, 2008; Glancy and Bell, 2000; Berti and Simoni, 2005; Larsen *et al.*, 2006; Godt and Coe, 2007). Coe *et al.* (2008) reported that the initiation via the fire-hose effect is controlled by the sediment supply, rather than by the moisture level.

In the Westfjords, Decaulne and Sæmundsson (2006) link the presence of release scars to debris flows originated by rotational slides. In Ísafjörður, debris-flow tracks 1DF and 2DF – not of new formation as 11DF and 12DF, but already formed at the time of the surveys – have curved release scarps showing signs of regressive erosion, ephemeral springs at the contact between loose debris and bedrock, erosion in the upper catchment (subareas 1DFa and 2DFa), and a main depositional area in the chute (subareas 1DFb and 2DFb). These are all evidence of slope failure, which through rotational sliding eroded material in the upper catchments and dammed the chutes depositing up to 3000 m^3 of debris at high slope angles (>35°). The slope failure process in this case has generated the preparatory conditions for future debris flows to occur. It is improbable that the deposits currently located in the chutes remain stable.

In particular, we believe that the debris-flow tracks 1DF and 2DF show the preparatory conditions for the fire-hose effect. 54.7% and 81.3%, respectively, of the overall deposited volumes in 1DF and 2DF are gathered in the chutes. It has been observed that hundreds to a few thousand cubic metres of loose

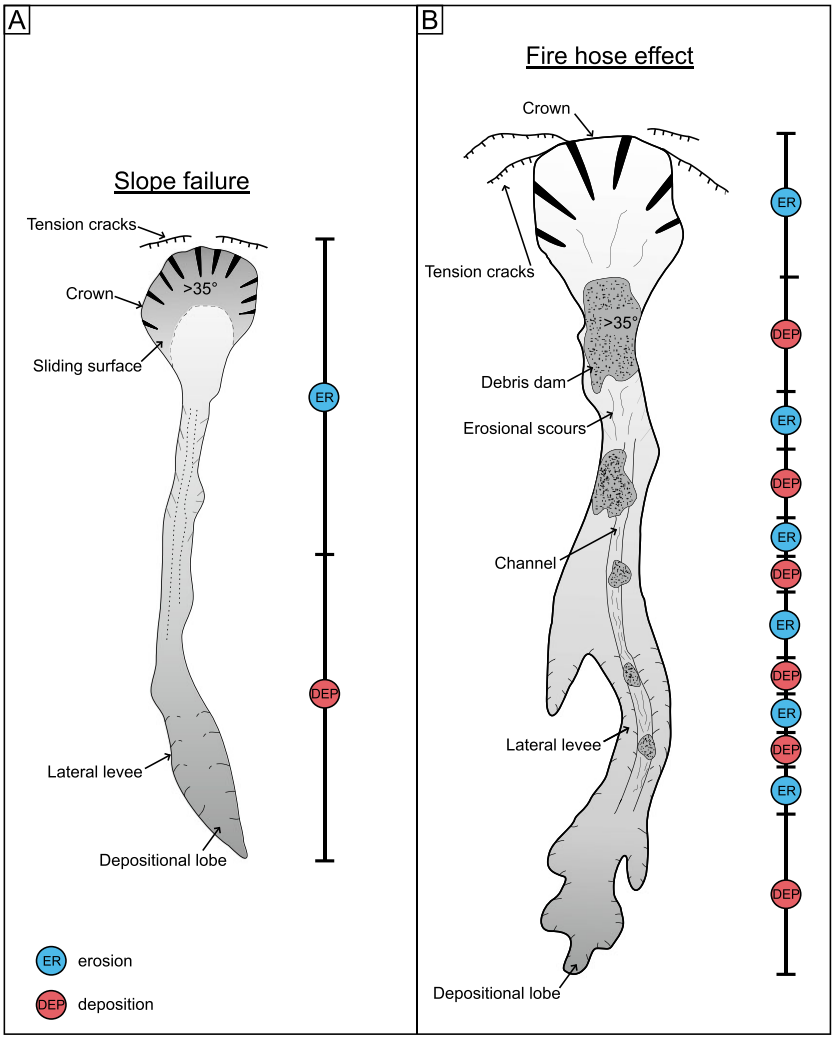

Figure 8. Simplified sketch of the main geomorphological characteristics of the slope failure (A) and the fire-hose effect (B). [Colour figure can be viewed at wileyonlinelibrary.com]

deposits reflects pulses of sediment supply from upslope catchments (Theule *et al.*, 2015), and that these pulses can be induced and fed by processes such as rockfalls (Loye *et al.*, 2016). Cascades of processes leading to slope failure have been observed in the field and in experiments, where surface water runoff causes erosion and accumulation of material, subsequently mobilised by shallow slides. Depending on the topography, sediment can be re-accumulated and periodically released as a debris-flow surge when impinged on by water flow (Kean *et al.*, 2013; Hu *et al.*, 2016).

Debris flows can be initiated by saturation and breaching of dams of sediment located in channels. We suggest that 1DF and 2DF tracks show a favourable setting to the fire-hose effect, since scarp failure and sediment storage are present in the chutes and channels. We hypothesise that some of the accumulated debris has probably already been transported downslope by the fire-hose effect. This is suggested by a trend of alternating zones of erosion and deposition throughout the 1DF and 2DF tracks and at different scales in the different subareas (Figure 8(B)). For example, in the lower parts (1DFc and 2DFc) of debris-flow tracks 1DF and 2DF, small zones of deposition and erosion are aligned within the channel, and along the central steepest path in the upper catchments and apical chutes, particularly clearly in 1DFa (Figures 4(B), 5(B)). We infer that this setting cannot be due to the failure of pre-existing material, such the collapse of lateral levees or lateral banks (Frank *et al.*, 2015; Hu *et al.*, 2016), as in the DoD, erosion of these features would be visible in correspondence with deposition in the chute or the channel. Therefore, we interpret these alternating zones of erosion and deposition to be likely the result of the transport of debris by the fire-hose effect: this has caused instantaneous sediment entrainment, as the build-up of the lateral levees occurs in association with discrete erosion zones in the chutes and channels (potential impact points; Coe *et al.*, 2008). The presence of these fire-hose events is also supported by the erosion volume being larger than the deposited one (i.e. debris has left the survey zone).

In Table IV, we compare our volume calculations with the volume results obtained by Decaulne *et al.* (2005) and Conway *et al.* (2010). Our deposition results for 1DF (4079 ± 223 m^3) and 2DF (3760 ± 127 m^3) are similar to those of Conway *et al.* (2010): 8287 m^3 and 1925 m^3, respectively, for the same tracks. The deposition value calculated for debris flow 2DF by Decaulne *et al.* (2005) matches fairly well with our calculation, but the event described by these authors extended to the base of the slope. In our study, much of the total deposited volumes for 1DF and 2DF lies in the chutes (1DFb with 2234 ± 21 m^3 and 2DFb with 3058 ± 30 m^3 in Table IV), rather than along the tracks, or in the depositional lobes as measured by Decaulne *et al.* (2005) and Conway *et al.* (2010). These volumes are of the same order of magnitude as the material mobilised by a debris flow in 1999 (estimated at 3000 m^3 for 2DF; Decaulne *et al.*, 2005) and from 1999 to 2007 (1925 m^3 for 2DF; Conway *et al.*, 2010). Previous studies (Glade, 2005; Decaulne and Sæmundsson, 2006; Conway *et al.*, 2010) recognised debris flows that had originated through the fire-

Table IV. Data regarding the debris flows described in this study, compared with the data of Conway *et al.* (2010) and Decaulne *et al.* (2005)

Debris flow ID	Years of activity	Years of data collections and authors	Method of survey	Estimated deposition m^3 (standard error)	Deposition m^3 (relative uncertainty) - This study	Estimated erosion m^3 (standard error)	Erosion m^3 (relative uncertainty) - This study
1DF	June 2006, 2007-2013	Summer 2007, Summer 2008: Conway et al. (2010)	LiDAR/airborne photographs, DGPS	8000 (±66%)	–	41000 (±38%)	–
		Summer 2007, Summer 2013: This study	LiDAR/airborne photograph	–	4079 (±5%)	–	-8552 (±4%)
2DF	1965, June 1999, June 2006, 2007-2013	Summer 1999: Decaulne et al. (2005)	Aerial photographs, field survey	3000	–	–	–
		Summer 2007, Summer 2008: Conway et al. (2010)	LiDAR/airborne photographs, DGPS	2000 (±134%)	–	16000 (±62%)	–
		Summer 2007, Summer 2013: This study	LiDAR/airborne photographs	–	3760 (±3%)	–	-5000 (±4%)
11DF	2007-2013	Summer 2007, Summer 2013: This study	LiDAR/airborne photographs	–	339 (±9%)	–	-862 (±5%)
12DF	2007-2013	Summer 2007, Summer 2013: This study	LiDAR/airborne photographs	–	271 (±11%)	–	-628 (±7%)

hose effect in other areas of the Westfjords in Iceland, but with a lower frequency (~10 years return) than the mean return period of Gleiðarhjalli area (4–5 years; Decaulne *et al.*, 2005). Those previous studies considered the fire-hose effect to only involve smaller volumes of material (700–1000 m^3), based on debris collected in the chutes by weathering and erosion of the bedrock (i.e. those flows are most likely supply-limited). Since 2007, much larger volumes gathered in the chutes of 1DF and 2DF tracks (subareas 'b') at high slope angle (~37–38°, see Figure 6). This setting is vulnerable to the fire-hose effect, and shows high potential mobility of the debris in the chutes of the 1DF and 2DF tracks.

Summary of debris-flow initiation processes identified in Ísafjörður

We have shown that the use of differenced LiDAR datasets for volume change detection, integrated with slope and geomorphic analysis from remote sensing data, and demonstrate its potential for identifying debris-flow initiation processes. The deposits in the chutes described by us would be 'invisible' in the datasets of Conway *et al.* (2010) and Decaulne *et al.* (2005), since in their field-based studies they could not quantify the material in the chutes of the flows. Our approach of identifying pre- and post-events changes in topography, volumes, slopes and morphology allowed us to distinguish between the slope failure initiation process and the formation of preparatory conditions for the fire-hose effect without having to witness them, making possible a discrimination that would have been virtually impossible otherwise.

The slope failure and the fire-hose effect as initiating processes for debris flows in the Westfjords were previously only hypothesised (Decaulne *et al.*, 2005; Decaulne and Sæmundsson, 2006; Conway *et al.*, 2010). The comparison of airborne datasets with a 6-year separation shows that the four debris-flow tracks analysed are geomorphically distinctive (see Figure 8) and show two different modes of flow initiation and evolution:

(1) Slope failure is the mechanism that triggered the newly-developed debris flow 11DF and 12DF, and that caused erosion in the upper catchments and deposit transfer in the chutes of the already-formed 1DF and 2DF tracks.
(2) We have been able to quantify the magnitudes of the volumes of material stored within debris-flow chutes and tracks above Ísafjörður by slope failure: this has produced debris dams at high slope angle, forming the preparatory conditions for the fire-hose effect. Part of this debris has probably already been transported by this mechanism. The large volumes of material stored in the chutes and channels of 1DF and 2DF (2000–3000 m^3 in subareas 1DFb and 2DFb) in the past were probably moved in a single sudden event, so they provide a substantial amount of material that could be mobilised by the fire-hose effect, leading to potentially hazardous debris flows, as cyclic damming has been proved to enlarge the size of new debris-flow pulses (Hu *et al.*, 2016). This further suggests that this repeated storage of large volumes of sediment in the upper parts of the slope could result in longer runout debris-flow tracks, compared to smaller flows that are formed by single slope failures.

Implications for potential mobility and hazard

In general, slope angles exceeding 20°–40° are sufficient for the development of slides in dry conditions, and these values can

be much lower in saturated conditions, depending on the nature of the material (Anderson and Anderson, 2010). Mean values of slope angles in 2013 in the upper zones of all the analysed debris flows are high (Table III; 36° in 1DFa, 38° in 2DFa, 37° in 11DFa, 41° in 12DFa). Instead of decreasing since 2007, the slope angle in the scarp zones is maintained, hence prone to new slides. We also found such high angles in other debris-flow chutes along the slope above Ísafjörður (Figure 9). Over an area of 0.55 km^2 defined along the edge of the bench, we calculated that ~17% is occupied by deposits perched on slopes exceeding 35° and ~4% exceeding 45°. This means that all these areas could be prone to failures.

In geomorphologic studies, the mobility of gravitational movements has been related to the volume and angle of repose (Corominas, 1996; Rickenmann, 1999; Legros, 2002; Toyos *et al.*, 2008). Steep slopes and initial failure volume have previously been shown to be important factors with respect to debris-flow initiation (Bovis and Dagg, 1992; Iverson, 1997; Brayshaw and Hassan, 2009). Steep channels are intrinsically less stable than low-angle channels, thus debris-flow initiation is more likely. In addition, large sediment volumes – which can self-increase as they travel downslope if runoff-initiated, as with fire-hose or sediment bulking (Godt and Coe, 2007) – usually travel at a higher flow speed than small failures when they enter the channel. Large volumes acquiring high speed are also more likely to impinge catastrophically on saturated deposits stored in the channel, triggering a further debris flow. Furthermore, the incision of the channel can progressively increase the volume of the flow during different debris-flow surges, with further material supplied in the flow by processes like channel scouring (Rickenmann and Zimmermann, 1993; Berti *et al.*, 1999; Hungr *et al.*, 2005). For these reasons, deeply incised pre-existing tracks like 1DF and 2DF in Ísafjörður are a further source of instability for the material upslope, and constitute a preferential path for sediment delivery downstream.

A high mobility debris flow, such as those that could be initiated by the fire-hose mechanism in tracks 1DF and 2DF, poses a potential hazard to people and property. The construction of new engineering solutions (in Figure 10 barriers A, 4A and 4B realised with gabions) and the improvement of old ones (barrier 3) to protect Ísafjörður from debris flows and snow avalanches were commissioned in 2012 (Municipality of Ísafjörður; report in Icelandic) and constitute a substantial improvement to the risk mitigation of the town. Old barrier 3 has been raised from 3 m to 5 m, while the new ones reach heights of up to 14 m. As barriers A and 3 are positioned beneath debris flow 2DF, they have the potential to retain a new flow in this track. However, there is no protection apart from the ditch beneath debris flow 1DF, whose terminal lobe deposits are located just 90 m above the main road (Figure 10).

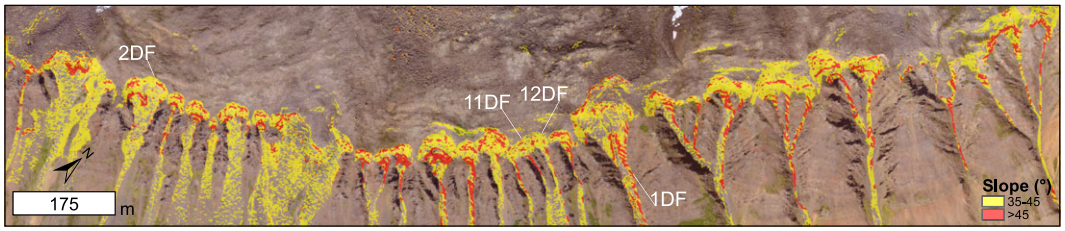

Figure 9. Slope map calculated from DEM 2013, showing loose deposits with angle higher than 35° and 45°. [Colour figure can be viewed at wileyonlinelibrary.com]

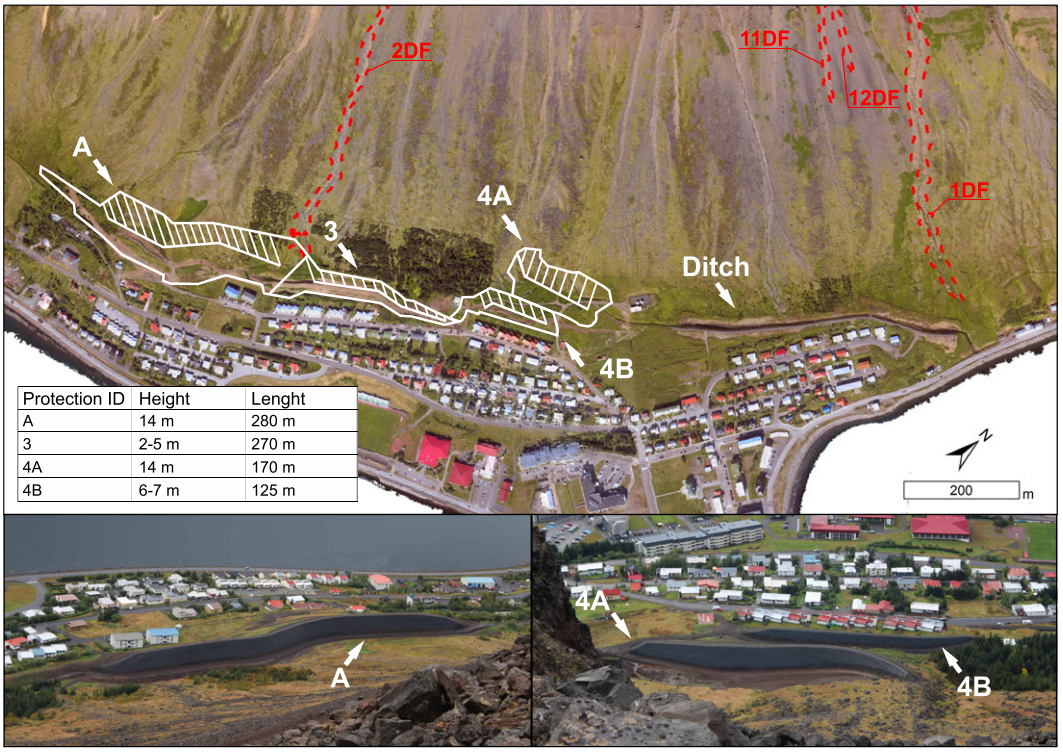

Figure 10. Plan of the snow avalanche and debris-flow protection measures ordered by the municipality of Ísafjörður in 2011 (protection measures have the same naming protocol used in the report in Icelandic from the municipality). Ditch and barrier 3 were already present in 2013 (ditch 2–3 m deep, barrier 3 3 m high). Dashed red line marks the perimeter of studied debris flows. [Colour figure can be viewed at wileyonlinelibrary.com]

The presence of these engineering solutions suggests that previous studies contributed to planning the measures of hazard mitigation for the town of Ísafjörður. Further efforts should be made in understanding debris-flow initiation, as the reliance of runout distance, flow volume, and return period for debris flows on their initial triggering mechanisms has broad implications for assessment of debris-flow hazards.

Finally, we note that the high quality topography data that can be obtained from airborne LiDAR surveys can be effectively used for hazard-monitoring purposes, but they are expensive and time-consuming to process. In this perspective, the use of unmanned aerial systems (UAS) able to collect topography data (usually from photogrammetry) and remote sensing images has been proven a valuable resource for high-resolution hazard surveys (Mancini *et al.*, 2013; Lucieer *et al.*, 2014; Jordan and Napier, 2015), and could be used as a data source for the same kind of analyses that we describe here. Annual UAS surveys of the debris-flow tracks above Ísafjörður could provide a flexible, cost-effective, and time efficient method for monitoring their evolution, especially the build-up of deposits in unstable parts of long tracks located above inhabited areas. Such data would also provide an important scientific resource for furthering the study of debris-flow initiation and evolution.

Conclusions

We have compared two airborne datasets (LiDAR topography and aerial images), collected in 2007 and 2013, that describe debris flows above the town of Ísafjörður in Iceland. This multi-temporal high-resolution approach reveals details about debris-flow processes in the steepest source areas that previous studies using traditional survey techniques (Decaulne *et al.*, 2005; Conway *et al.*, 2010) were unable to fully analyse. Our main conclusions are:

(a) Slope failure of the deposits from the edge of the Gleiðarhjalli bench is the dominant initiation process, leading to a new generation of debris-flow landforms above the town (11DF and 12DF) and mobilising debris now in transit in the chutes and upper channels of pre-existing tracks (1DF and 2DF). The fire-hose effect could re-activate older flows (1DF and 2DF), and has probably already mobilised debris within their channels.
(b) The two mechanisms can be geomorphologically distinguished, with slope failure characterised by a simple upper–lower erosion–deposition pattern, defined scarps with possible regressive erosion, steep (>35°) discrete slide surfaces with ephemeral springs, modest (below 1000 m^3) mobilised volumes, and short-runout. Preparatory conditions for the fire-hose effect-triggered debris flows are discrete zones of deposited material at high angle (>35°) in the chute and along the channel, and alternating zones of fill and scour along their whole length.
(c) Volumes of debris stored in the chutes and upper channels of medium-scale debris-flow tracks 1DF and 2DF (2200–3000 m^3) are stored at high angles (37–38°) and have the same order of magnitude as those estimated for single damaging events that happened in the past (Decaulne *et al.*, 2005; Conway *et al.*, 2010). We infer that these two debris dams have high potential mobility. This confirms hypotheses previously suggested (but not confirmed directly, nor precisely quantified) by Decaulne *et al.* (2005) and Conway *et al.* (2010) – namely that there are large volumes of material blocking steep channels in Ísafjörður.

More widely, we have shown that our geomorphic criteria applied on LiDAR differencing has permitted us to detect, quantify and characterise debris accumulated at high gradients, without the assistance of any other monitoring system or information on the evolution of the debris flow and of their triggering conditions. The slope of Ísafjörður is extremely prone to activation and re-activation of debris flows, so this kind of study in this and other debris-flow threatened areas, supported by *in situ* channel survey and monitoring, can improve our understanding of both how debris flows develop and how to mitigate the risks associated with them.

Acknowledgements—This work would not have been possible without a postgraduate studentship grant (NE/L002493/1) from the CENTA Doctoral Training Partnership funded by the UK Natural Environment Research Council (NERC) and the British Geological Survey University Funding Initiative Studentship (GA/14S/024, Ref: 284). We thank the NERC Airborne Research Facility Data Analysis Node for obtaining the aerial photography and LiDAR data, for the airborne survey project NERC ARSF 07217a in 2007 and for the airborne survey project NERC ARSF IG13-11 in 2013. We thank the NERC Geophysical Equipment Facility for technical support and for the loan number 1001. We would like to show our gratitude to Jón Kristinn Helgason (Icelandic Meteorological Office), who provided expertise that greatly improved the manuscript. We acknowledge constructive comments and suggestions from two anonymous reviewers. C. Jordan publishes with permission from the Executive Director of the British Geological Survey.

Conflict of Interest

The authors declare no competing interests.

References

Akca D. 2007. *Least Squares 3D Surface Matching*. Zurich: Eidgenössische Technische Hochschule Zürich.

Anderson RS, Anderson SP. 2010. *Geomorphology: the Mechanics and Chemistry of Landscapes*. Cambridge University Press: Cambridge.

Anderson SA, Sitar N. 1995. Analysis of rainfall-induced debris flows. *Journal of Geotechnical Engineering* **121**: 544–552. https://doi.org/10.1061/(ASCE)0733-9410(1995)121:7(544).

Bangen S, Hensleish J, McHugh P, Wheaton J. 2016. Error modeling of DEMs from topographic surveys of rivers using fuzzy inference systems. *Water Resources Research* **52**: 1176–1193. https://doi.org/10.1002/2014WR015716.

Berti M, Genevois R, Simoni A, Tecca PR. 1999. Field observations of a debris flow event in the Dolomites. *Geomorphology* **29**: 265–274. https://doi.org/10.1016/S0169-555X(99)00018-5.

Berti M, Simoni A. 2005. Experimental evidences and numerical modelling of debris flow initiated by channel runoff. *Landslides* **2**: 171–182. https://doi.org/10.1007/s10346-005-0062-4.

Besl P, McKay N. 1992. A method for registration of 3-D shapes. *IEEE Transactions on Pattern Analysis and Machine Intelligence* **14**: 239–256. https://doi.org/10.1109/34.121791.

Blasone G, Cavalli M, Marchi L, Cazorzi F. 2014. Monitoring sediment source areas in a debris-flow catchment using terrestrial laser scanning. *Catena* **123**: 23–36. https://doi.org/10.1016/j.catena.2014.07.001.

Bossi G, Cavalli M, Crema S, Frigerio S, Quan Luna B, Mantovani M, Marcato G, Schenato L, Pasuto A. 2015. Multi-temporal LiDAR-DTMs as a tool for modelling a complex landslide: a case study in the Rotolon catchment (eastern Italian Alps). *Natural Hazards and Earth System Sciences* **15**: 715–722. https://doi.org/10.5194/nhess-15-715-2015.

Bovis M, Jones P. 1992. Holocene history of earthflow mass movements in south-central British Columbia: the influence of hydroclimatic changes. *Canadian Journal of Earth Sciences* **29**: 1746–1755.

Bovis MJ, Dagg BR. 1992. Debris flow triggering by impulsive loading: mechanical modelling and case studies. *Canadian Geotechnical Journal* **29**: 345–352.

Brasington J, Langham J, Rumsby B. 2003. Methodological sensitivity of morphometric estimates of coarse fluvial sediment transport.

Geomorphology **53**: 299–316. https://doi.org/10.1016/S0169-555X(02)00320-3.

Brasington J, Rumsby BT, Mcvey RA. 2000. Monitoring and modelling morphological change in a braided gravel-bed river using high resolution Gps. *Earth Surface Processes and Landforms* **25**: 973–990. https://doi.org/10.1002/1096-9837(200008)25:9<973::AID-ESP111>3.0.CO;2-Y.

Brayshaw D, Hassan MA. 2009. Debris flow initiation and sediment recharge in gullies. *Geomorphology* **109**: 122–131. https://doi.org/10.1016/j.geomorph.2009.02.021.

Bremer M, Sass O. 2012. Combining airborne and terrestrial laser scanning for quantifying erosion and deposition by a debris flow event. *Geomorphology* **138**: 49–60. https://doi.org/10.1016/j.geomorph.2011.08.024.

Bull JM, Miller H, Gravley DM, Costello D, Hikuroa DCH, Dix JK. 2010. Assessing debris flows using LIDAR differencing: 18 May 2005 Matata event, New Zealand. *Geomorphology* **124**: 75–84. https://doi.org/10.1016/j.geomorph.2010.08.011.

Burrough PA, McDonnell RA, Lloyd CD. 2015. *Principles of Geographical Information Systems*. Oxford University Press: Oxfrod.

Campbell RH. 1975. Soil slips, debris flows, and rainstorms in the Santa Monica mountains and vicinity, Southern California. *US Geological Survey Professional Paper* **851**: 51.

Cannon SH, Kirkham RM, Parise M. 2001. Wildfire-related debris-flow initiation processes, Storm King Mountain, Colorado. *Geomorphology* **39**: 171–188. https://doi.org/10.1016/S0169-555X(00)00108-2.

Cavalli M, Goldin B, Comiti F, Brardinoni F, Marchi L. 2017. Assessment of erosion and deposition in steep mountain basins by differencing sequential digital terrain models. *Geomorphology* **291**: 4–16. https://doi.org/10.1016/j.geomorph.2016.04.009.

Chen Y, Medioni G. 1992. Object modelling by registration of multiple range images. *Image and Vision Computing* **10**: 145–155.

Coe JA, Glancy PA, Whitney JW. 1997. Volumetric analysis and hydrologic characterization of a modern debris flow near Yucca Mountain, Nevada. *Geomorphology* **20**: 11–28. https://doi.org/10.1016/S0169-555x(97)00008-1.

Coe JA, Kinner DA, Godt JW. 2008. Initiation conditions for debris flows generated by runoff at Chalk Cliffs, central Colorado. *Geomorphology* **96**: 270–297. https://doi.org/10.1016/j.geomorph.2007.03.017.

Conway SJ, Decaulne A, Balme MR, Murray JB, Towner MC. 2010. A new approach to estimating hazard posed by debris flows in the Westfjords of Iceland. *Geomorphology* **114**: 556–572. https://doi.org/10.1016/j.geomorph.2009.08.015.

Corominas J. 1996. The angle of reach as a mobility index for small and large landslides. *Canadian Geotechnical Journal* **33**: 260–271.

Costa JE. 1984. Physical Geomorphology of Debris Flows. In *Developments and Applications of Geomorphology*, Costa JE, Fleisher PJ (eds). Springer: Berlin, Heidelberg.

Curry RR. 1966. Observation of alpine mudflows in the Tenmile Range, central Colorado. *Geological Society of America Bulletin* **77**: 771–776.

Davies TRH. 1986. Large debris flows: a macro-viscous phenomenon. *Acta Mechanica* **63**: 161–178.

Decaulne A. 2004. Combining geomorphological, historical and lichenometrical data for assessment of risk due to present-day slope processes, a case study from the Icelandic Westflords. In *Risk Analysis IV*, Brebbia CA (ed). Wit Press: Southampton; 177–186.

Decaulne A. 2005. Slope processes and related risk appearance within the Icelandic Westfjords during the twentieth century. *Natural Hazards and Earth System Science* **5**: 309–318. https://doi.org/10.5194/nhess-5-309-2005.

Decaulne A, Sæmundsson Þ. 2003. Debris-flows characteristics in the Gleidarhjalli area, North-western Iceland. In *Debris-Flow Hazards Mitigation: Mechanics, Prediction, and Assessment*, Rickenmann D, Chen CL (eds). Mill Press: Rotterdam: Davos, Switzerland; 1107–1118.

Decaulne A, Sæmundsson Þ. 2006. Geomorphic evidence for present-day snow-avalanche and debris-flow impact in the Icelandic Westfjords. *Geomorphology* **80**: 80–93. https://doi.org/10.1016/j.geomorph.2005.09.007.

Decaulne A, Sæmundsson Þ. 2007. Spatial and temporal diversity for debris-flow meteorological control in subarctic oceanic periglacial environments in Iceland. *Earth Surface Processes and Landforms* **32**: 1971–1983. https://doi.org/10.1002/esp.1509.

Decaulne A, Sæmundsson P, Pétursson O. 2005. Debris flow triggered by rapid snowmelt: a case study in the Gleidarhjalli area, northwestern Iceland. *Geografiska Annaler, Series A: Physical Geography* **87**: 487–500. https://doi.org/10.1111/j.0435-3676.2005.00273.x.

Elwell HA, Stocking MA. 1976. Vegetal cover to estimate soil erosion hazard in Rhodesia. *Geoderma* **15**: 61–70. https://doi.org/10.1016/0016-7061(76)90071-9.

Fairchild LH. 1987. The importance of lahar initiation processes. *Reviews in Engineering Geology* **7**: 51–62.

Favalli M, Fornaciai A, Pareschi MT. 2009. LIDAR strip adjustment: application to volcanic areas. *Geomorphology* **111**: 123–135. https://doi.org/10.1016/j.geomorph.2009.04.010.

Frank F, McArdell BW, Huggel C, Vieli A. 2015. The importance of entrainment and bulking on debris flow runout modeling: examples from the Swiss Alps. *Natural Hazards and Earth System Sciences* **15**: 2569–2583. https://doi.org/10.5194/nhess-15-2569-2015.

Fryxell FM, Horberg L. 1943. Alpine mudflows in Grand Teton National Park, Wyoming. *Geological Society of America Bulletin* **54**: 457–472.

Fuller IC, Large ARG, Charlton ME, Heritage GL, Milan DJ. 2003. Reach-scale sedime nt transfers: an evaluation of two morphological budgeting approaches. *Earth Surface Processes and Landforms* **28**: 889–903. https://doi.org/10.1002/esp.1011.

Glade T. 2005. Linking debris-flow hazard assessments with geomorphology. *Geomorphology* **66**: 189–213. https://doi.org/10.1016/j.geomorph.2004.09.023.

Glancy P, Bell JW. 2000. Landslide-induced flooding at Ophir Creek, Washoe County, western Nevada, May 30, 1983. US Geological Survey Professional Paper 1617

Godt JW, Coe JA. 2007. Alpine debris flows triggered by a 28 July 1999 thunderstorm in the central Front Range, Colorado. *Geomorphology* **84**: 80–97. https://doi.org/10.1016/j.geomorph.2006.07.009.

Goulden T, Hopkinson C. 2010. The forward propagation of integrated system component errors within airborne Lidar data. *Photogrammetric Engineering and Remote Sensing* **76**: 589–601. https://doi.org/10.14358/PERS.76.5.589.

Griffiths PG, Webb RH. 2004. Frequency and initiation of debris flows in Grand Canyon, Arizona. *Journal of Geophysical Research* **109**: 1–14. https://doi.org/10.1029/2003JF000077.

Hu W, Dong XJ, Xu Q, Wang GH, van Asch TWJ, Hicher PY. 2016. Initiation processes for run-off generated debris flows in the Wenchuan earthquake area of China. *Geomorphology* **253**: 468–477. https://doi.org/10.1016/j.geomorph.2015.10.024.

Hungr O, Evans SG, Bovis MJ, Hutchinson JN. 2001. A review of the classification of landslides of the flow type. *Environmental and Engineering Geoscience* **7**: 221–238. https://doi.org/10.2113/gseegeosci.7.3.221.

Hungr O, Leroueil S, Picarelli L. 2014. The Varnes classification of landslide types, an update. *Landslides* **11**: 167–194. https://doi.org/10.1007/s10346-013-0436-y.

Hungr O, McDougall S, Bovis M. 2005. Entrainment of material by debris flows. In *Debris-Flow Hazards and Related Phenomena*. Springer: Berlin/Heidelberg; 135–158.

Hürlimann M, Rickenmann D, Graf C. 2003. Field and monitoring data of debris-flow events in the Swiss Alps. *Canadian Geotechnical Journal* **40**: 161–175. https://doi.org/10.1139/t02-087.

Imaizumi F, Sidle RC, Tsuchiya S, Ohsaka O. 2006. Hydrogeomorphic processes in a steep debris flow initiation zone. *Geophysical Research Letters* **33**: 2–5. https://doi.org/10.1029/2006GL026250.

Innes JL. 1983. Debris flows. *Progress in Physical Geography* **7**: 469–501.

Iverson RM. 1997. The physics of debris flows. *Review of Geophysics* **3**: 245–296.

Iverson RM, Denlinger RP, LaHusen RG, Logan M. 2000. Two-phase debris flow across 3-D terrain: Model predictions and experimental tests. In *Debris-Flow Hazards Mitigation: Mechanics, Prediction, and Assessment*, vol. 2, Wieczorek GF, Naeser ND (eds). A. A. Balkema: Brookfield, Vt; 521–529.

James MR, Robson S. 2014. Mitigating systematic error in topographic models derived from UAV and ground-based image networks. *Earth Surface Processes and Landforms* **39**: 1413–1420. https://doi.org/10.1002/esp.3609.

Johnson AM, Rodine JR. 1984. Debris flow. In *Slope Instability*, Brunsden D, Prior DB (eds). Wiley: Chichester; 257–361.

Jordan CJ, Napier B. 2015. Developing digital fieldwork technologies at the British Geological Survey. *Geological Society, London, Special Publications* **436**: 1–11. https://doi.org/10.1144/SP436.6.

Kean JW, McCoy SW, Tucker GE, Staley DM, Coe JA. 2013. Runoff-generated debris flows: observations and modeling of surge initiation, magnitude, and frequency. *Journal of Geophysical Research: Earth Surface* **118**: 2190–2207. https://doi.org/10.1002/jgrf.20148.

Kristjánsson L, Pätzold R, Preston J. 1975. The palaeomagnetism and geology of the Patreksfjördur-Arnarfjördur region of Northwest Iceland. *Tectonophysics* **25** (3-4): 201–216. https://doi.org/10.1016/0040-1951(75)90027-X.

Lane SN, Westaway RM, Hicks DM. 2003. Estimation of erosion and deposition volumes in a large, gravel-bed, braided river using synoptic remote sensing. *Earth Surface Processes and Landforms* **28**: 249–271. https://doi.org/10.1002/esp.483.

Larsen IJ, Pederson JL, Schmidt JC. 2006. Geologic versus wildfire controls on hillslope processes and debris flow initiation in the Green River canyons of Dinosaur National Monument. *Geomorphology* **81**: 114–127. https://doi.org/10.1016/j.geomorph.2006.04.002.

Legros F. 2002. The mobility of long-runout landslides. *Engineering Geology* **63**: 301–331. https://doi.org/10.1016/S0013-7952(01)00090-4.

Loye A, Jaboyedoff M, Isaac Theule J, Liébault F. 2016. Headwater sediment dynamics in a debris flow catchment constrained by high-resolution topographic surveys. *Earth Surface Dynamics* **4**: 489–513. https://doi.org/10.5194/esurf-4-489-2016.

Lucieer A, Jong SM d, Turner D. 2014. Mapping landslide displacements using Structure from Motion (SfM) and image correlation of multi-temporal UAV photography. *Progress in Physical Geography* **38**: 97–116. https://doi.org/10.1177/0309133313515293.

Mancini F, Dubbini M, Gattelli M, Stecchi F, Fabbri S, Gabbianelli G. 2013. Using unmanned aerial vehicles (UAV) for high-resolution reconstruction of topography: the structure from motion approach on coastal environments. *Remote Sensing* **5**: 6880–6898. https://doi.org/10.3390/rs5126880.

Marchi L, Arattano M, Deganutti AM. 2002. Ten years of debris-flow monitoring in the Moscardo Torrent (Italian Alps). *Geomorphology* **46**: 1–17. https://doi.org/10.1016/S0169-555X(01)00162-3.

McArdell BW, Bartelt P, Kowalski J. 2007. Field observations of basal forces and fluid pore pressure in a debris flow. *Geophysical Research Letters* **34**: 2–5. https://doi.org/10.1029/2006GL029183.

Micheletti N, Chandler JH, Lane SN. 2015. Investigating the geomorphological potential of freely available and accessible structure-from-motion photogrammetry using a smartphone. *Earth Surface Processes and Landforms* **40**: 473–486. https://doi.org/10.1002/esp.3648.

Milan DJ, Heritage GL, Hetherington D. 2007. Application of a 3D laser scanner in the assessment of erosion and deposition volumes and channel change in a proglacial river. *Earth Surface Processes and Landforms* **32**: 1657–1674. https://doi.org/10.1002/esp.

Moss JL. 2000. Using the Global Positioning System to monitor dynamic ground deformation networks on potentially active landslides. *International Journal of Applied Earth Observation and Geoinformation* **2**: 24–32. https://doi.org/10.1016/S0303-2434(00)85023-0.

Municipality of Ísafjörður. 2012. Ofanflóðavarnir neðan Gleiðarhjalla á ÍsafirðiOfanflóðavarnir neðan Gleiðarhjalla á Ísafirði. Mat á umhverfisáhrifum Matsskýrsla.

Reuter HI, Hengl T, Gessler P, Soille P. 2009. Preparation of DEMs for geomorpometric analysis. *Developments in Soil Science* **33**: 87–120. https://doi.org/10.1016/S0166-2481(08)00004-4.

Rickenmann D. 1999. Empirical relationships for debris flows. *Natural Hazards* **19**: 47–77. https://doi.org/10.1023/A:1008064220727.

Rickenmann D, Koschni A. 2010. Sediment loads due to fluvial transport and debris flows during the 2005 flood events in Switzerland. *Hydrological Processes* **24**: 993–1007. https://doi.org/10.1002/hyp.7536.

Rickenmann D, Zimmermann M. 1993. The 1987 debris flows in Switzerland: documentation and analysis. *Geomorphology* **8**: 175–189.

Roberti G, Ward B, van Wyk de Vries B, Friele P, Perotti L, Clague JJ, Giardino M. 2017. Precursory slope distress prior to the 2010 Mount Meager landslide, British Columbia. *Landslides* **15** (4): 1–11. https://doi.org/10.1007/s10346-017-0901-0.

Rodolfo KS, Umbal JV, Alonso RA, Remotigue CT, Paladio-Melosantos ML, Salvador JH, Evangelista D, Miller Y. 1996. Two years of lahars on the western flank of Mount Pinatubo: initiation, flow processes, deposits, and attendant geomorphic and hydraulic changes. In *Fire and Mud: Eruptions and lahars of Mount Pinatubo, Philippines*, Newhall CG, Punongbayan RS (eds); 989–1013.

Sæmundsson K. 1980. Outline of the geology of Iceland. *Jökull* **29**: 7–28.

Sæmundsson Þ, Pétursson HG, Decaulne A. 2003. Triggering factors for rapid mass movements in Iceland. In *Debris-Flow Hazards Mitigation: Mechanics, Prediction, and Assessment*, Rickenman D, Chen CI (eds). Mill Press: Rotterdam; 167–178.

Schaffrath KR, Belmont P, Wheaton JM. 2015. Landscape-scale geomorphic change detection: quantifying spatially variable uncertainty and circumventing legacy data issues. *Geomorphology* **250**: 334–348. https://doi.org/10.1016/j.geomorph.2015.09.020.

Scheidl C, Rickenmann D, Chiari M. 2008. The use of airborne LiDAR data for the analysis of debris flow events in Switzerland. *Natural Hazards and Earth System Science* **8**: 1113–1127. https://doi.org/10.5194/nhess-8-1113-2008.

Sidle RC, Swanston DN. 1982. Analysis of a small debris slide in coastal Alaska. *Canadian Geotechnical Journal* **19**: 167–174.

Sofia G, Pirotti F, Tarolli P. 2013. Variations in multiscale curvature distribution and signatures of LiDAR DTM errors. *Earth Surface Processes and Landforms* **38**: 1116–1134. https://doi.org/10.1002/esp.3363.

Terzaghi K, Peck R, Mesri G. 1996. *Soil Mechanics in Engineering Practice*. 3rd edition. John Wiley & Sons: New York.

Theule JI, Liébault F, Laigle D, Loye A, Jaboyedoff M. 2015. Channel scour and fill by debris flows and bedload transport. *Geomorphology* **243**: 92–105. https://doi.org/10.1016/j.geomorph.2015.05.003.

Theule JI, Liébault F, Loye A, Laigle D, Jaboyedoff M. 2012. Sediment budget monitoring of debris-flow and bedload transport in the Manival Torrent, SE France. *Natural Hazards and Earth System Science* **12**: 731–749. https://doi.org/10.5194/nhess-12-731-2012.

Thordarson T, Hoskuldsson A. 2002. Iceland. In *Classic Geology in Europe 3*. Terra Publishing: Harpenden, UK.

Toyos G, Gunasekera R, Zanchetta G, Oppenheimer C, Sulpizio R, Favalli M, Pareschi MT. 2008. GIS-assisted modelling for debris flow hazard assessment based on the events of May 1998 in the area of Sarno, Southern Italy: II. Velocity and dynamic pressure. *Earth Surface Processes and Landforms* **33**: 1693–1708. https://doi.org/10.1002/esp.1640.

Wells WG. 1981. Some effects of brushfires or erosion processes in coastal southern California. In *Erosion and Sediment Transport in Pacific-Rim Steeplands*, Vol. **132**, Proceedings of the Christchurch Symposium. International Association of Hydrological Sciences: Christchurch, New Zealand, January 25–31 ; 305–342.1981

Wells WG. 1987. The effects of fire on the generation of debris flows in southern California. *Reviews in Engineering Geology* **7**: 105–114.

Wheaton JM, Brasington J, Darby SE, Sear DA. 2010. Accounting for uncertainty in DEMs from repeat topographic surveys: improved sediment budgets. *Earth Surface Processes and Landforms* **35**: 136–156. https://doi.org/10.1002/esp.1886.

Wieczorek GF, Glade T. 2005. Climatic factors influencing occurrence of debris flows. In *Debris-Flow Hazards and Related Phenomena*, Jakob M, Hungr O (eds). Springer: Berlin; 325–362.

Zhang Z. 1994. Iterative point matching for registration of free-form curves and surfaces. *International Journal of Computer Vision* **13**: 119–152. https://doi.org/10.1007/BF01427149.

